

A Comparative Study for Single Image Blind Deblurring

Wei-Sheng Lai¹ Jia-Bin Huang² Zhe Hu¹ Narendra Ahuja² Ming-Hsuan Yang¹
¹University of California, Merced ²University of Illinois, Urbana-Champaign

http://vllab.ucmerced.edu/~wlai24/cvpr16_deblur_study

Abstract

Numerous single image blind deblurring algorithms have been proposed to restore latent sharp images under camera motion. However, these algorithms are mainly evaluated using either synthetic datasets or few selected real blurred images. It is thus unclear how these algorithms would perform on images acquired “in the wild” and how we could gauge the progress in the field. In this paper, we aim to bridge this gap. We present the first comprehensive perceptual study and analysis of single image blind deblurring using real-world blurred images. First, we collect a dataset of real blurred images and a dataset of synthetically blurred images. Using these datasets, we conduct a large-scale user study to quantify the performance of several representative state-of-the-art blind deblurring algorithms. Second, we systematically analyze subject preferences, including the level of agreement, significance tests of score differences, and rationales for preferring one method over another. Third, we study the correlation between human subjective scores and several full-reference and no-reference image quality metrics. Our evaluation and analysis indicate the performance gap between synthetically blurred images and real blurred image and sheds light on future research in single image blind deblurring.

1. Introduction

The recent years have witnessed significant progress in single image blind deblurring (or motion deblurring). The progress in this field can be attributed to the advancement of efficient inference algorithms [2, 5, 17, 35, 44], various natural image priors [15, 21, 29, 38, 45], and more general motion blur models [8, 9, 11, 43]. To quantify and compare the performance of competing algorithms, existing methods either use (1) synthetic datasets [17, 38] with uniform blurred images generated by convolving a sharp image with a known blur kernel, or (2) a non-uniform blurred benchmark [13] constructed by recording and playing back camera motion in a lab setting. However, existing datasets do not consider several crucial factors, e.g., scene depth variation, sensor saturation and nonlinear camera response func-

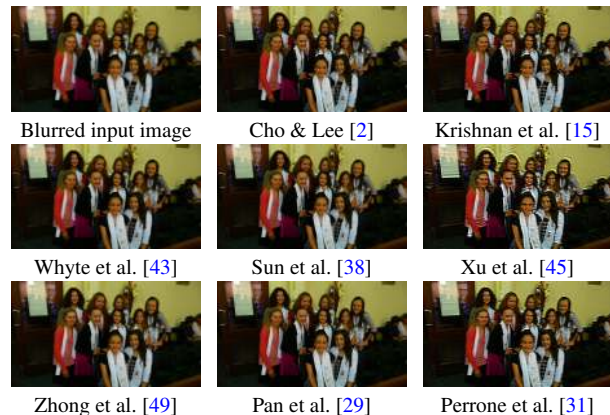


Figure 1. A blurred image from the real dataset proposed in this work and a few deblurred results from state-of-the-art algorithms, where there is no clear winner. In this work, we aim to evaluate the performance of single image deblurring algorithms on the *real-world* blurred images by human perceptual studies.

tions in a camera pipeline. To understand the true progress of deblurring algorithms, it is important to evaluate the performance “in the wild”. While several work has reported impressive results on real blurred images, the lack of a large benchmark dataset and perceptual comparison makes it impossible to evaluate the relative strengths of these algorithms in the literature.

There are two main drawbacks in existing evaluation approaches. First, the synthetically generated blurred images often fail to capture the complexity and the characteristics of real motion blur degradation. For example, the camera motion has 6 degrees of freedom (3 translations and 3 rotations) while a convolution model considers only 2D translations parallel to the image plane [17, 38]. Lens distortion, sensor saturation, nonlinear transform functions, noise, and compression in a camera pipeline are also not taken into account in these synthetically generated images. Furthermore, the constant scene depth assumption in a convolution model and the non-uniform blurred benchmark [13] may not hold in many real scenes where the depth variation cannot be neglected. Evaluations on these datasets do not reflect the performance of single image blind deblurring algorithms on the

Table 1. Existing and the proposed datasets for performance evaluation of single image blind deblurring algorithms. The proposed dataset consists of both synthetic and real blurred images. Our real dataset contains real blurred images that cover a wide variety of scenarios. Our synthetic dataset includes both uniform and non-uniform blurred images.

Dataset	Levin et al. [17]	Sun et al. [38]	Köhler et al. [13]	Ours (real)	Ours (synthetic)
Synthetic/Real	Synthetic	Synthetic	Real	Real	Synthetic
Blur Model	Uniform	Uniform	Non-uniform	Unknown	Both
Latent Images	4	80	4	100	25
Kernels / Trajectories	8	8	12	100	8
Blurred Images	32	640	48	100	200
Depth variation	No	No	No	Yes	No
Evaluation	PSNR/SSIM	PSNR/SSIM	PSNR	User study	User study

real-world images. Second, existing methods use PSNR and SSIM to quantify performance, which do not correlate well with human perception in image deblurring [20]. The lack of human perceptual studies makes it difficult to compare the performance of deblurring algorithms. While numerous full-reference [36, 37] and no-reference image quality metrics [19, 23, 24, 26, 27, 33, 47] have been proposed, it is unclear whether these metrics can be applied to measure the quality of deblurred images.

In this paper, we propose a comparative study of single image blind deblurring algorithms to address these issues. First, we construct two large datasets: (1) real blurred images and (2) synthetic motion-blurred images. We annotate these images with attributes including man-made, natural, people/face, saturated, and text. Second, we conduct a large-scale user study to compare state-of-the-art single image blind deblurring algorithms (see Figure 1 for an example of deblurred results from several state-of-the-art algorithms). The statistical analysis of different image attributes helps understand the performance of algorithms in a systematic manner. Third, by comparing our user study results between the real and synthetic datasets, we gain insights that cannot be inferred from the original publications, including image priors, blur models, evaluated datasets and quality metrics (See Section 5).

The contributions of this work are threefold:

- **Datasets.** We construct two large datasets for evaluating image deblurring algorithms: (1) real blurred images and (2) synthetically blurred images. Our real dataset contains real blurred images captured under different scenarios. Our synthetic dataset includes both uniform and non-uniform motion-blurred images.
- **Human subject evaluation.** We evaluate 13 state-of-the-art single image motion deblurring algorithms, including uniform and non-uniform deblurring, with a large-scale perceptual user study. We show the performance gap when we evaluate these algorithms on synthetic and real images.
- **Quality metric comparison.** We compare the performance of several full-reference and no-reference image quality metrics on both synthetic and real datasets.

2. Related Work

Datasets and benchmarks. Several datasets have been used to measure and compare the performance of image deblurring algorithms. Levin et al. [17] construct a dataset with four latent sharp images and eight uniform blur kernels, resulting in total 32 test images. However, the four gray-scale latent images with spatial resolution of 255×255 pixels are not sufficient to cover a wide variety of real-world scenarios. Sun et al. [38] extend the dataset by using 80 high-resolution natural images of diverse scenes and synthetically blurring each one with the eight blur kernels from [17]. To construct a non-uniform blur dataset, Köhler et al. [13] record 6D camera trajectories over time, and play back the camera motion on a robotic platform to capture blurred images. This benchmark contains four latent images and 12 camera trajectories. However, similar to [17], the scene is assumed planar and at a fixed distance from the camera. While the PSNR and SSIM metrics are widely used for evaluating the performance of image deblurring algorithms [13, 17, 38], these measures do not match human perception very well [20]. In contrast, our real dataset contains 100 real-world blurred images, and our synthetic dataset has 200 synthetic blurred images with both uniform and non-uniform blur. The latent images in our datasets cover various scenarios and represent the actual challenges and variations in the real world. Table 1 lists the comparison between the proposed and existing datasets. We describe more details in Section 3.1.

Human perceptual study. As many commonly used quantitative metrics do not reflect human perceptual preferences, large-scale user studies have been used to evaluate the performance based on visual perception in several computational photography problems. Examples include tone mapping [16], image retargeting [32], and single image super resolution [46]. To obtain the ranking of the evaluated algorithms, a straightforward way is to show all deblurred results simultaneously for a subject to rank. However, such an approach is neither feasible nor accurate when there exist a large number of test images and algorithms to be evaluated. Thus, prior work often adopts paired comparison in

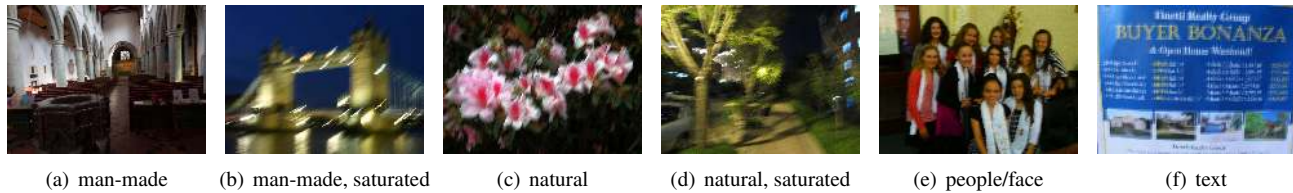


Figure 2. Sample images with the annotated attributes in our real dataset. The numbers of images belonging to each attribute in our real dataset are: man-made (66), natural (14), people/face (12), saturated (28), and text (17).

a user study, where subjects are asked to choose a preference between two results (i.e., partial order), instead of giving unreliable scores or rankings for comparing multiple results. We note that Liu et al. [20] also conduct a user study to obtain subjective perceptual scores for image deblurring. Our work differs from [20] in three major aspects. First, the goal of [20] is to learn a no-reference metric from the collected perceptual scores while our objective is the performance comparison of state-of-the-art deblurring algorithms on the real-world images. Second, unlike [20] where synthetic uniform blurred images are used, our real dataset better reflects the complexity and variations of blurred images in the real world. Third, we evaluate both uniform and non-uniform deblurring algorithms while the focus of [20] is on algorithms addressing uniform blur only.

3. Experimental Settings

3.1. Image Datasets

Real image dataset. In this paper, we aim to evaluate the performance of deblurring algorithms for real blurred images “in the wild”. To this end, we construct a set of 100 real blurred images via multiple sources, e.g., representative images from previous work [2, 5, 43, 44], images from Flickr and Google Image Search, or pictures captured by ourselves. All these blurred images are captured in the real-world scenarios from different cameras (e.g., consumer cameras, DSLR, or cellphone cameras), different settings (e.g., exposure time, aperture size, ISO), and different users. We categorize images according to the following five attributes: man-made, natural, people/face, saturated, and text. Figure 2 shows sample images along with these main attributes. To make these images computationally feasible for most deblurring algorithms, we resize each image such that the maximum dimension is less than 1200 pixels.

Synthetic dataset. To examine the performance consistency between real and synthetic images, we collect 25 sharp images from the Internet as ground truth and synthesize 100 non-uniform and 100 uniform blurred images. We label these images using the above-mentioned five attributes with each group having at least five images. To synthesize non-uniform blurred images, we record the 6D camera trajectories using a cellphone with inertial sensors (gyroscope

and accelerometer), and construct a collection of spatially varying blur kernels by assuming constant depth for the scenes. We obtain the 100 non-uniform blurred images by applying four camera trajectories to 25 latent images and adding 1% Gaussian noise to simulate camera noise. As the sizes of local blur kernels are less than 25×25 , we set the support size to 25×25 when deblurring those non-uniform blurred images. For uniform blur, the eight blur kernels provided by Levin et al. [17] have been used in several datasets [28, 29, 38]. However, the maximum blur kernel size of these eight blur kernels is 41×41 , which is relatively small in the real-world cases. We thus use the algorithm in [34] to synthesize blur kernels by sampling random 6D camera trajectories, generating four uniform blur kernels with size ranging from 51×51 to 101×101 . We then use a convolution model with 1% Gaussian noise to synthesize the 100 uniform blurred images. We present our uniform and non-uniform blur kernels in the supplementary material. We create the synthetic saturated images in a way similar to [3, 10]. Specifically, we first stretch the intensity range of the latent image from $[0, 1]$ to $[-0.1, 1.8]$, and convolve the blur kernels with the images. We then clip the blurred images into the range of $[0, 1]$. The same process is adopted for generating non-uniform blurred images.

3.2. Evaluated Algorithms

We evaluate deblurring algorithms with publicly available source code or binary executable. We evaluate 13 representative state-of-the-art algorithms [2, 5, 15, 18, 21, 29, 31, 38, 43, 44, 45, 48, 49] in our experiments¹. We include the input blurred images in the evaluation as well. Table 2 shows the list of evaluated algorithms.

We fix the support size of the blur kernel for each evaluated algorithm when estimating a blur kernel from a test image. For fair comparisons, we use the default parameter values and apply the same non-blind deconvolution method [14] with the estimated kernels to obtain the final deblurred results. However, the method [14] fails to handle images with large saturated regions. In Figure 3(a), we show an example where the non-blind deconvolution

¹While the method [48] is designed for multi-image blind deconvolution, it can be applied to single images as well. As the non-uniform method [45] on the project website does not work stably for large blur kernels, we use the uniform deblurring code of [45] requested from the author.

Table 2. List of evaluated algorithms. We present a complete table with image priors, blur kernel priors and the execution time of all evaluated algorithms in the supplementary material.

Algorithm	Blur Model	Algorithm	Blur Model
Fergus-06 [5]	Uniform	Xu-13 [45]	Uniform
Cho-09 [2]	Uniform	Zhang-13 [48]	Uniform
Xu-10 [44]	Uniform	Zhong-13 [49]	Uniform
Krishnan-11 [15]	Uniform	Michaeli-14 [21]	Uniform
Levin-11 [18]	Uniform	Pan-14 [29]	Uniform
Whyte-12 [43]	Non-uniform	Perrone-14 [31]	Uniform
Sun-13 [38]	Uniform		



(a) kernel [29] + nonblind [14] (b) kernel [29] + nonblind [42]

Figure 3. Deblurring saturated images with fast non-blind deconvolution [14] and non-blind deconvolution with saturation handling [42].

method [14] results in serious ringing artifacts. To address this issue, we adopt the non-blind deconvolution algorithm [42] that explicitly handles saturated regions when reconstructing the test images with this attribute. Figure 3(b) shows the deblurred result by using [42] for non-blind deconvolution. We note that the some methods [17, 21, 42, 44] fail to estimate large blur kernels in about 0.5% of all test images. We exclude these failure cases from our evaluation.

3.3. Human Subject Study

We conduct our experiments using Amazon Mechanical Turk for large-scale subject studies to evaluate the performance of single image blind deblurring algorithms. We adopt the paired comparison approach that requires each human subject to choose a preferred image from a pair of deblurred images. We design a website that allows each subject to flip between two deblurred images and easily examine the differences. We show a screenshot of the user interface in the supplementary material. There are 14 result images (13 deblurred images and 1 blurred input) for each test image in our datasets. The total number of pair comparisons is $\binom{14}{2} \times 100 = 9100$. In a user study session, we ask each subject to compare 50 pairs of images. To remove careless comparisons by the subjects, we introduce sanity check by adding several image pairs where one image is considerably better than the other. For the real dataset, we manually select some pairs of well-deblurred images and images containing severe ringing artifacts or noise. For the synthetic dataset, we use the pairs of ground-truth latent and blurred images. Among the 50 pairs of images for each subject, we select 10 pairs for a sanity check. We discard the voting results by a subject if the subject fails the sanity check more than once. We collect the results of human sub-

ject studies from 2,100 users. The average time to complete a survey is 15 minutes. We discard 1.45% of the votes (from subjects who fail to pass the sanity check).

4. Evaluation and Analysis

In this work, we aim to evaluate the performance of single image blind deblurring algorithms based on human visual perception. In addition to ranking the algorithms, we exploit the correlation between the real and synthetic datasets, as well as the performance of image quality metrics on predicting the quality of deblurred images. First, we analyze the degree of agreement [12] among subjects to make sure that the votes are not random. Second, we fit paired comparison results to the Bradley-Terry model [1] to obtain a global score and rank for each algorithm. We analyze the convergence of ranking to show that the number of votes and images in our human subject study are sufficient to draw solid conclusions. We also conduct a significance test [6] to group the evaluated algorithms based on perceptual quality (that are statistically indistinguishable). Finally, we show the correlation between human perceptual scores and existing image quality metrics.

4.1. Coefficient of Agreement

While we rule out noisy votes with the use of sanity check, the votes may appear random if the participants' preferences are dramatically different. We thus study the similarity of choices (i.e., the degree of agreement) among subjects. We apply the Kendall coefficient of agreement [12] to quantify the level of agreement with u :

$$u = \frac{2W}{\binom{S}{2} \binom{M}{2}} - 1, \quad W = \sum_{i \neq j} \binom{c_{ij}}{2}, \quad (1)$$

where c_{ij} is the number of times that method i is chosen over method j , S denotes the number of subjects, and M represents the number of compared methods. If all subjects make the same choice for each comparison, then the Kendall coefficient of agreement u is equal to 1. The minimum value of u is $-1/S$, indicating evenly distributed answers. For example, suppose that there are 100 subjects answering one binary preference question (choice of A or B, assuming A is better than B). The Kendall coefficient of agreement $u = 0.1$ if there are 67 subjects choosing A over B, and $u = 0.2$ if there are 73 subjects choosing A over B. If 50 subjects vote for A and 50 subjects vote for B, u attains the minimum value of -0.01 .

In our evaluation, we randomly select pairs of deblurred images and ask the subjects' preference. As a result, we balance the subject votes by uniformly sampling the paired comparisons so that all the evaluated methods are compared at the same frequency. In Figure 4, we show the Kendall coefficients of the agreement under different attributes. The

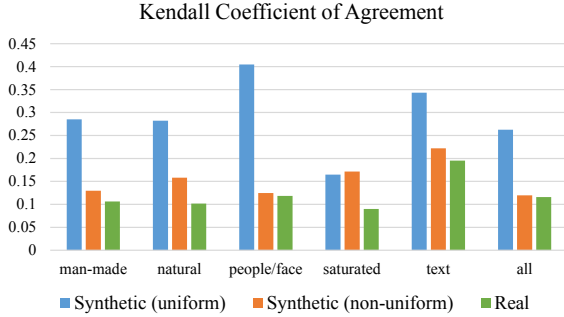


Figure 4. Kendall coefficient of agreement under different attributes in our human subject study.

coefficients for both the real and the synthetic non-uniform datasets are all around 0.12. On the other hand, we observe a higher level of agreement for the synthetic uniform dataset ($u = 0.26$).

We note that many algorithms (e.g., [2, 17, 21, 48]) favor no-blur explanations for the test images in the synthetic non-uniform dataset. In such cases, subjects have to choose between two poorly deblurred images, which leads to inconsistent votes. For real blurred images, many factors (e.g., depth variation, nonlinear camera response functions, and unknown camera noise) affect the performance of deblurring algorithms. Existing algorithms often have difficulty in handling real blurred images as they do not take these factors into considerations. In many test images, there is no clear winner. As a result, the degree of agreement in the real dataset is relatively low. We observe that the coefficients of agreement for text images on both the real and the synthetic datasets are higher than other attributes. One possible reason is that human subjects prefer sharp text images (as they are easier to read). The high contrast of the deblurred text images makes the comparisons less ambiguous.

4.2. Global Ranking

To compute the global ranking from paired comparisons, we use the Bradley-Terry model (B-T model) [1]: a probability model that predicts the outcome of the paired comparison. We denote $\mathbf{s} = [s_1, s_2, \dots, s_M]$ as M scores of the evaluated methods. The B-T model assumes that the probability of choosing method i over method j is:

$$p_{ij} = \frac{e^{s_i}}{e^{s_i} + e^{s_j}}. \quad (2)$$

Since each pair of result (i, j) is compared by multiple subjects, the likelihood of i over j is defined as $p_{ij}^{c_{ij}}$, where c_{ij} is the number of times that method i is chosen over method j . The likelihood of all (i, j) pairs is:

$$P = \prod_{i=1}^M \prod_{\substack{j=1 \\ j \neq i}}^M p_{ij}^{c_{ij}}. \quad (3)$$

We can estimate the score s_i by minimizing the negative log likelihood of (3):

$$L(\mathbf{s}) = \sum_{i=1}^M \sum_{\substack{j=1 \\ j \neq i}}^M c_{ij} \log(e^{s_i} + e^{s_j}) - \sum_{i=1}^M \sum_{\substack{j=1 \\ j \neq i}}^M c_{ij} s_i. \quad (4)$$

We can easily solve the optimization problem by setting the derivative of (4) to zero. We note that there is an ambiguity in the computed scores \mathbf{s} that cannot be determined by solving (4). That is, adding a constant δ to all s_i does not change the objective value. Thus, we normalize the B-T scores by shifting the scores to zero mean after solving (4).

Ranking. We rank the evaluated methods by the average B-T scores, and plot the cumulative frequency of B-T scores in Figure 5. We show the complete ranking results on different attributes in the supplementary material. In Figure 5, the method with the rightmost curve has a better overall performance because it has more images with higher B-T scores. In addition to the performance evaluation, we analyze the correlation of B-T scores between each pair of datasets as shown in Figure 6. The performance of those methods located in the lower-right corner of the figure is *over-estimated* on the dataset shown on the x -axis. On the other hand, the performance of those methods located in the upper-left corner is *under-estimated*. Take Figure 6(a) as an example. The methods [38, 44, 45] outperform all the other algorithms on the synthetic uniform dataset. However, their performances on the real dataset are not as competitive, e.g., the results from [29, 15] achieves higher scores than that of [38, 44, 45]. In this case, performance of [38, 44, 45] is over-estimated and the performance of [29, 15] is under-estimated on the synthetic uniform dataset. Therefore, the evaluation results based on synthetic uniform images do not well reflect the performance on the real-world images. In Figure 6(b), we observe that the performance of deblurring algorithms are similar on the real and the synthetic non-uniform datasets.

Convergence analysis. We analyze the convergence of global ranking on (1) the number of subject votes and (2) the number of test images to ensure that the number of votes and images are sufficiently large for performance evaluation. We randomly sample $k = 500, 1000, 2000, 3000, 4000$ votes from a total of 23,478 voting results in the real dataset and compute the B-T scores for each evaluated algorithm. We repeat this process 1000 times with different sample of votes. Figure 7(a) shows the mean and standard deviation for each k . At the beginning ($k = 500$), the error bars of these methods overlap with each other. When $k \geq 2000$, the standard deviations become sufficiently small, and the B-T scores of each method converge.

We conduct a similar analysis regarding the number of images. We randomly sample k ($k = 5, 10, 20, 30, 40$) images out of a total of 100 images from our real dataset,

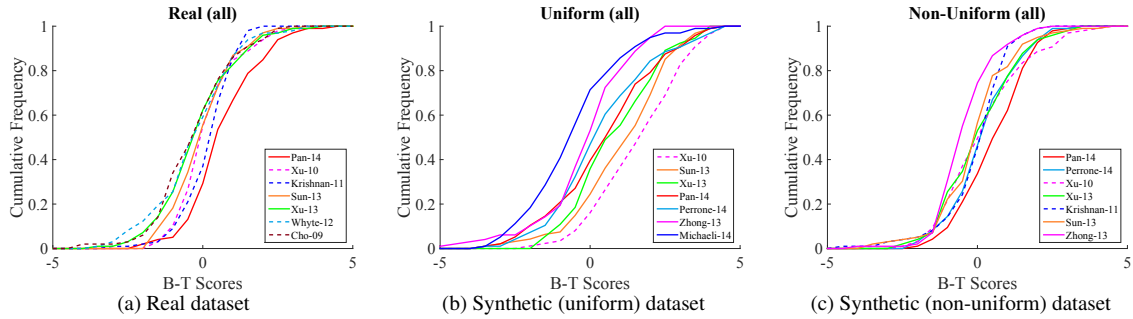


Figure 5. Cumulative frequency of B-T scores for each dataset. We normalize the frequency such that the maximum frequency is equal to 1. The method whose curve locates at right has more images with higher scores, which stands for better overall performance. Only the top 7 methods are presented for clarity. The complete plots of all evaluated methods are illustrated in the supplementary material.

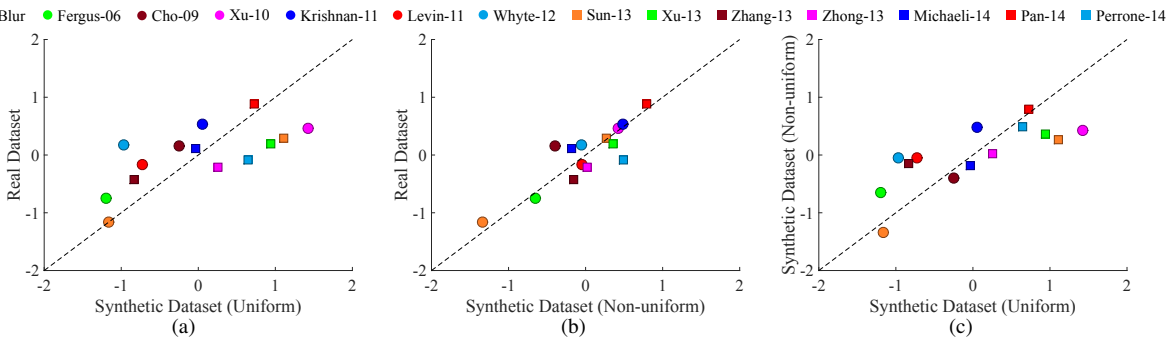


Figure 6. Correlation of B-T scores between a pair of datasets. The performance of those methods located in the lower-right is over-estimated on the dataset shown on the x -axis, while the performance of the methods located in the upper-left is under-estimated.

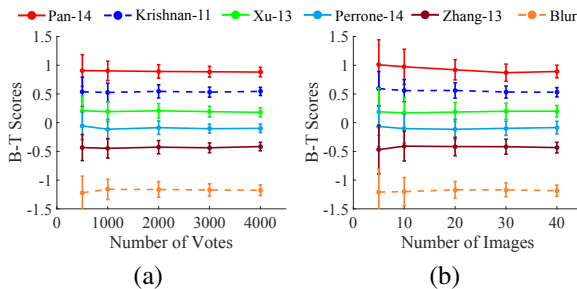


Figure 7. Convergence analysis on B-T scores with respect to the number of votes and the number of images.

and then plot the means and the standard deviations in Figure 7(b). The error-bars become sufficiently small to separate each evaluated method after using 30 images. These two experiments demonstrate that the number of votes and the number of test images are indeed sufficient to obtain stable scores or ranks.

4.3. Significance Test

An algorithm having a higher B-T score does not mean that it always outperforms others. To investigate whether the results of the evaluated methods are statistically distinguishable, we conduct the significance test [6] for each dataset. Specifically, we group the evaluated methods if the difference of obtained votes between any two methods within a group is less than a threshold.

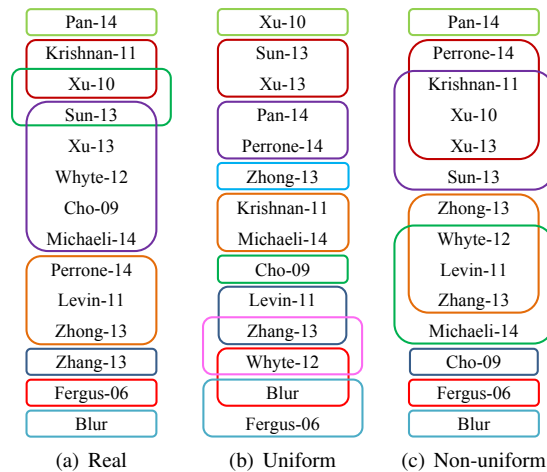


Figure 8. Grouping of algorithms by the significance test. Algorithms within the same circle have statistically indistinguishable scores, i.e., the performance is similar.

We denote the difference of the number of votes within a group of methods as R . We aim to find a threshold R' such that the probability $P[R \geq R'] \leq \alpha$, where α is the significance level ($\alpha = 0.01$ in this work). Since the distribution of R is asymptotically equivalent to the distribution of the variance-normalized range W_r [7], we can use the following

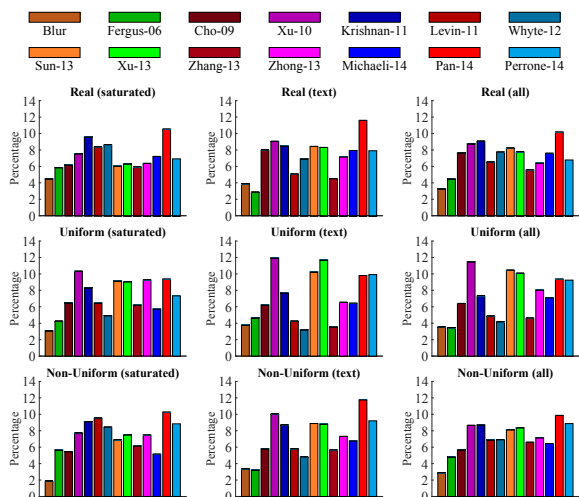


Figure 9. Percentage of obtained votes (y-axis) per attribute in each dataset. We show the full results of all five attributes in the supplementary material.

relationship to approximate $P[R \geq R']$:

$$P[W_M \geq W_{M,\alpha}] \leq \alpha \quad \text{where} \quad W_{M,\alpha} = \frac{2R' - 0.5}{\sqrt{MS}}. \quad (5)$$

In $W_{M,\alpha}$, M is the number of evaluated methods and S is the number of subjects. The value of $W_{M,\alpha}$ can be obtained from the table in [30], or one can draw M samples from a Gaussian distribution with variance 1 and then compute the upper $(1 - \alpha) \times 100$ percentage points as $W_{M,\alpha}$. Once we determine the value of $W_{M,\alpha}$, we can solve the value of R' using:

$$R' = 0.5W_{M,\alpha}\sqrt{MS} + 0.25. \quad (6)$$

A group is formed if and only if the score difference of any pair within a group is less or equal to R' . Otherwise, these two methods belong to different groups.

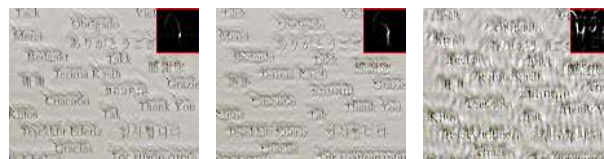
Table 3 lists the total number of votes, the number of comparisons for each pair (i, j) , and the value of R' used in each dataset. We show the ranking and the grouping results in Figure 8. The top three groups are different in the real and synthetic datasets. This suggests that the performance of a deblurring algorithm on synthetic images does not correlate well with the performance on real-world blurred images. In Figure 9, we also show the percentage of obtained votes. For avoiding clutter, we only show the results on images with the saturated and text attributes. We refer the readers to the supplementary material for the complete results for all attributes.

From the experimental results, we have a few interesting observations:

1. Krishnan-11 [15] performs worse in the synthetic dataset but better than most of algorithms in the real dataset. We attribute this observation to the fact that the deblurred results of Krishnan-11 usually contain

Table 3. Total number of votes, number of comparisons for each pair (i, j) , and value of threshold R' used in the significance test, where the significance level $\alpha = 0.01$.

	Real Dataset	Synthetic Dataset	
		Uniform	Non-uniform
votes	23478	23478	22750
comparisons	258	258	250
threshold R'	163	163	156



(a) Krishnan et al. [15] (b) Xu et al. [45] (c) Perrone et al. [31]

Figure 10. Human subjects often favor slightly blurry results with less ringing artifacts or over-sharpened edges (e.g., [15]).

fewer artifacts, e.g., serious ringings or over-sharpened edges. Figure 1 and Figure 10 show the deblurred results of Krishnan-11 compared to recent work.

2. Since most uniform deblurring algorithms do not handle non-uniform blurred images well, the results from many of the deblurring algorithms are statistically indistinguishable. However, some uniform deblurring algorithms [15, 29, 38, 44] are more robust than the non-uniform deblurring algorithm [43] in the synthetic non-uniform dataset and real dataset. Our empirical observations agree with the findings in [13].
3. Although Pan-14 [29] is designed to deblur text images, it performs well on real blurred images, particularly for saturated ones. The L_0 intensity prior used in Pan-14 favors images which have more pixels with zero intensity, and thus can reduce light streaks and saturated regions. In addition, Xu-10 [44] can deblur images with large motion blur in the presence of noise. The refinement phase in Xu-10 helps reduce noise in blur kernels and leads to robust deblurring results.

4.4. Analysis on Image Quality Metrics

In this section, we analyze the correlation between human subject scores and several image quality metrics. For full-reference metrics, we choose several widely used metrics, PSNR and SSIM [40], as well as WSNR [22], MS-SSIM [41], IFC [37], NQM [4], UIQI [39], VIF [36]. For no-reference metrics, we choose seven state-of-the-art no-reference metrics including BIQI [26], BLIINDS2 [33], BRISQUE [23], CORNIA [47], DIIVINE [27], NIQE [24], SSEQ [19]² and the no-reference metric for motion deblurring [20]. In total, there are eight full-reference metrics and eight no-reference metrics in our experiment. We com-

²Note that the score used in BIQI, BLIINDS2, BRISQUE, CORNIA, DIIVINE, NIQE and SSEQ range from 0 (best) to 100 (worst), and we reverse the score to make the correlation consistent to other quality metrics.

Table 4. Spearman’s rank correlation coefficient [25] of full-reference metrics (top 8) and no-reference metrics (bottom 8).

	Real Dataset	Synthetic Dataset	
		Uniform	Non-uniform
PSNR	-	0.4135	0.0819
WSNR [22]	-	0.4669	0.1662
SSIM [40]	-	0.5162	0.1511
MS-SSIM [41]	-	0.6385	0.2204
IFC [37]	-	0.6773	0.3132
NQM [4]	-	0.5394	0.1422
UIQI [39]	-	0.6282	0.2127
VIF [36]	-	0.5779	0.3366
BIQI [26]	0.0622	-0.0528	-0.1218
BLIINDS2 [33]	-0.0614	-0.0461	-0.1078
BRISQUE [23]	-0.0556	-0.0857	-0.1316
CORNIA [47]	0.0967	0.2630	0.0765
DIIVINE [27]	0.0284	-0.0805	-0.0017
NIQE [24]	0.0776	0.0110	-0.0308
SSEQ [19]	-0.0120	-0.0331	0.0212
Liu et al. [20]	0.1667	0.4991	0.2928

pute the Spearman’s rank correlation coefficient (denoted by ρ) [25], which measures the level of association between a pair of ranked variables. Note that Spearman’s rank correlation coefficient is not affected by the range of variables. This is particularly suitable for our study as different metrics may have different ranges.

Table 4 shows the value of ρ for all evaluated image quality metrics on both real and synthetic datasets. For full-reference metrics (the top eight rows in Table 4), IFC and VIF have higher ρ values than PSNR and SSIM. We note that the IFC metric uses wavelet features with a focus on high-frequency details, and VIF puts more weight on image edges when extracting features. Thus, these two metrics have higher correlation on the synthetic dataset. However, the overall correlation of all full-reference metrics on the non-uniform dataset is lower than that on the uniform dataset. This can be attributed to the fact that most evaluated algorithms assume the uniform blur model, which is not effective for handling non-uniform blurred images. For no-reference metrics (bottom eight of Table 4), most of them have lower or even negative correlation to human subjective scores. We note that the metric for motion deblurring [20] has high correlation on the synthetic dataset because this metric is trained specifically to evaluate the image quality of deblurred results. However, the correlation becomes significantly lower in the real dataset. As the metric [20] is learned from a synthetic uniform dataset, it does not work well on real images which contain non-uniform blur.

In addition to these image quality metrics, we also compute the correlation between human subject scores and the error ratio [17], which is a commonly used metric for evaluating the quality of deblurred images. The Spearman’s rank correlation coefficient of the error ratio is 0.5941, which is lower than IFC (0.6773) but better than PSNR (0.4135) and SSIM (0.5162). The result suggests that the error ratio is

a fair metric to evaluate the quality of deblurred images. However, the error ratio can only be applied to synthetic uniform blurred images with known ground truth blur kernels.

5. Discussions and Conclusion

In this paper, we carry out large-scale experiments to evaluate the performance of state-of-the-art single image motion deblurring algorithms on both real and synthetic blurred datasets. From our evaluation and analysis, we present our observations and suggestions for future research with respect to the following issues.

Image priors: Sparse gradient priors [15] and intensity [29] are more reliable and effective than explicit edge-based methods [38, 44, 45] for real images. We attribute this to the heuristic edge selection steps, in which the thresholding parameters are sensitive to image contents and less robust to noise in real images. We observe that human subjects tend to prefer slightly blurry results to sharper results but with noticeable artifacts.

Blur models: Existing deblurring algorithms are less effective in dealing with saturated regions, non-Gaussian noise, and complicated scenes with large depth variation. We advocate putting more research attention on better model design to handle complex and non-uniform motion blur as well as image noise caused by outliers.

Datasets: From the study, we found that existing methods already perform well on synthetic images but not on real images. Similar to other fields in computer vision (e.g., object detection and recognition), the cumulative advances make this community ready to focus on development and evaluation on real images.

Quality metrics: IFC and VIF perform better than PSNR and SSIM when evaluating the quality of deblurred images on the synthetic dataset. For no-reference quality metrics, the motion deblurring metric [20] has a high correlation with human perceptual scores on the synthetic dataset, but less so on the real dataset.

Our datasets, subject votes and code for the statistical analysis in this paper are available on our project website. We encourage community to develop robust algorithms to account for practical scenarios and design image quality metrics to measure the performance of deblurring algorithms on real-world blurred images.

Acknowledgments

This work is supported in part by the NSF CAREER Grant #1149783, NSF IIS Grant #1152576, a gift from Adobe, Office of Naval Research N00014-12-1-0259, and Air Force Office of Scientific Research AF FA8750-13-2-0008.

References

- [1] R. A. Bradley and M. E. Terry. Rank analysis of incomplete block designs the method of paired comparisons. *Biometrika*, 39(3-4):324–345, 1952. 4, 5
- [2] S. Cho and S. Lee. Fast motion deblurring. *ACM TOG (Proc. SIGGRAPH Asia)*, 28(5):145:1–145:8, 2009. 1, 3, 4, 5
- [3] S. Cho, J. Wang, and S. Lee. Handling outliers in non-blind image deconvolution. In *ICCV*, 2011. 3
- [4] N. Damera-Venkata, T. D. Kite, W. S. Geisler, B. L. Evans, and A. C. Bovik. Image quality assessment based on a degradation model. *TIP*, 9(4):636–650, 2000. 7, 8
- [5] R. Fergus, B. Singh, A. Hertzmann, S. T. Roweis, and W. T. Freeman. Removing camera shake from a single photograph. *ACM TOG (Proc. SIGGRAPH)*, 25(3):787–794, 2006. 1, 3, 4
- [6] R. A. Fisher. Statistical methods for research workers. 1925. 4, 6
- [7] E. N. Gilbert. Review: H. A. David, The method of paired comparisons. *Ann. Math. Statist.*, 35(3):1386–1387, 1964. 6
- [8] A. Gupta, N. Joshi, C. L. Zitnick, M. Cohen, and B. Curless. Single image deblurring using motion density functions. In *ECCV*, 2010. 1
- [9] M. Hirsch, C. J. Schuler, S. Harmeling, and B. Schölkopf. Fast removal of non-uniform camera shake. In *ICCV*, 2011. 1
- [10] Z. Hu, S. Cho, J. Wang, and M.-H. Yang. Deblurring low-light images with light streaks. In *CVPR*, 2014. 3
- [11] Z. Hu, L. Xu, and M.-H. Yang. Joint depth estimation and camera shake removal from single blurry image. In *CVPR*, 2014. 1
- [12] M. G. Kendall and B. B. Smith. On the method of paired comparisons. *Biometrika*, 31(3-4):324–345, 1940. 4
- [13] R. Köhler, M. Hirsch, B. Mohler, B. Schölkopf, and S. Harmeling. Recording and playback of camera shake: Benchmarking blind deconvolution with a real-world database. In *ECCV*, 2012. 1, 2, 7
- [14] D. Krishnan and R. Fergus. Fast image deconvolution using hyper-laplacian priors. In *NIPS*, 2009. 3, 4
- [15] D. Krishnan, T. Tay, and R. Fergus. Blind deconvolution using a normalized sparsity measure. In *CVPR*, 2011. 1, 3, 4, 5, 7, 8
- [16] P. Ledda, A. Chalmers, T. Troscianko, and H. Seetzen. Evaluation of tone mapping operators using a high dynamic range display. *ACM TOG (Proc. SIGGRAPH)*, 24(3):640–648, 2005. 2
- [17] A. Levin, Y. Weiss, F. Durand, and W. T. Freeman. Understanding and evaluating blind deconvolution algorithms. In *CVPR*, 2009. 1, 2, 3, 4, 5, 8
- [18] A. Levin, Y. Weiss, F. Durand, and W. T. Freeman. Efficient marginal likelihood optimization in blind deconvolution. In *CVPR*, 2011. 3, 4
- [19] L. Liu, B. Liu, H. Huang, and A. C. Bovik. No-reference image quality assessment based on spatial and spectral entropies. *Signal Processing: Image Communication*, 29(8):856–863, 2014. 2, 7, 8
- [20] Y. Liu, J. Wang, S. Cho, A. Finkelstein, and S. Rusinkiewicz. A no-reference metric for evaluating the quality of motion deblurring. *ACM TOG (Proc. SIGGRAPH Asia)*, 32(6):175, 2013. 2, 3, 7, 8
- [21] T. Michaeli and M. Irani. Blind deblurring using internal patch recurrence. In *ECCV*, 2014. 1, 3, 4, 5
- [22] T. Mitsa and K. L. Varkur. Evaluation of contrast sensitivity functions for the formulation of quality measures incorporated in halftoning algorithms. In *ICASSP*, volume 5, pages 301–304, 1993. 7, 8
- [23] A. Mittal, A. K. Moorthy, and A. C. Bovik. No-reference image quality assessment in the spatial domain. *TIP*, 21(12):4695–4708, 2012. 2, 7, 8
- [24] A. Mittal, R. Soundararajan, and A. C. Bovik. Making a completely blind image quality analyzer. *IEEE Signal Processing Letters*, 20(3):209–212, 2013. 2, 7, 8
- [25] D. S. Moore and G. P. McCabe. Introduction to the practice of statistics. 1989. 8
- [26] A. K. Moorthy and A. C. Bovik. A two-step framework for constructing blind image quality indices. *IEEE Signal Processing Letters*, 17(5):513–516, 2010. 2, 7, 8
- [27] A. K. Moorthy and A. C. Bovik. Blind image quality assessment: From natural scene statistics to perceptual quality. *TIP*, 20(12):3350–3364, 2011. 2, 7, 8
- [28] J. Pan, Z. Hu, Z. Su, and M.-H. Yang. Deblurring face images with exemplars. In *ECCV*, 2014. 3
- [29] J. Pan, Z. Hu, Z. Su, and M.-H. Yang. Deblurring text images via l0-regularized intensity and gradient prior. In *CVPR*, 2014. 1, 3, 4, 5, 7, 8
- [30] E. S. Pearson and H. O. Hartley. *Biometrika tables for statisticians*. 1988. 7
- [31] D. Perrone and P. Favaro. Total variation blind deconvolution: The devil is in the details. In *CVPR*, 2014. 1, 3, 4, 7
- [32] M. Rubinstein, D. Gutierrez, O. Sorkine, and A. Shamir. A comparative study of image retargeting. *ACM TOG (Proc. SIGGRAPH Asia)*, 29(6):160:1–160:10, 2010. 2
- [33] M. A. Saad, A. C. Bovik, and C. Charrier. Blind image quality assessment: A natural scene statistics approach in the dct domain. *TIP*, 21(8):3339–3352, 2012. 2, 7, 8
- [34] U. Schmidt, C. Rother, S. Nowozin, J. Jancsary, and S. Roth. Discriminative non-blind deblurring. In *CVPR*, 2013. 3
- [35] Q. Shan, J. Jia, and A. Agarwala. High-quality motion deblurring from a single image. *ACM TOG (Proc. SIGGRAPH)*, 27(3):73, 2008. 1
- [36] H. R. Sheikh and A. C. Bovik. Image information and visual quality. *TIP*, 15(2):430–444, 2006. 2, 7, 8
- [37] H. R. Sheikh, A. C. Bovik, and G. De Veciana. An information fidelity criterion for image quality assessment using natural scene statistics. *TIP*, 14(12):2117–2128, 2005. 2, 7, 8
- [38] L. Sun, S. Cho, J. Wang, and J. Hays. Edge-based blur kernel estimation using patch priors. In *ICCP*, 2013. 1, 2, 3, 4, 5, 7, 8
- [39] Z. Wang and A. C. Bovik. A universal image quality index. *IEEE Signal Processing Letters*, 9(3):81–84, 2002. 7, 8
- [40] Z. Wang, A. C. Bovik, H. R. Sheikh, and E. P. Simoncelli. Image quality assessment: from error visibility to structural similarity. *TIP*, 13(4):600–612, 2004. 7, 8
- [41] Z. Wang, E. P. Simoncelli, and A. C. Bovik. Multiscale structural similarity for image quality assessment. In *Proceedings of Conference on Signals, Systems and Computers*, 2003. 7, 8
- [42] O. Whyte, J. Sivic, and A. Zisserman. Deblurring shaken and partially saturated images. *IJCV*, 110(2):185–201, 2014. 4
- [43] O. Whyte, J. Sivic, A. Zisserman, and J. Ponce. Non-uniform deblurring for shaken images. *IJCV*, 98(2):168–186, 2012. 1, 3, 4, 7
- [44] L. Xu and J. Jia. Two-phase kernel estimation for robust motion deblurring. In *ECCV*, 2010. 1, 3, 4, 5, 7, 8
- [45] L. Xu, S. Zheng, and J. Jia. Unnatural L_0 sparse representation for natural image deblurring. In *CVPR*, 2013. 1, 3, 4, 5, 7, 8
- [46] C.-Y. Yang, C. Ma, and M.-H. Yang. Single-image super-resolution: A benchmark. In *ECCV*, 2014. 2
- [47] P. Ye, J. Kumar, L. Kang, and D. Doermann. Unsupervised feature learning framework for no-reference image quality assessment. In *CVPR*, 2012. 2, 7, 8
- [48] H. Zhang, D. Wipf, and Y. Zhang. Multi-image blind deblurring using a coupled adaptive sparse prior. In *CVPR*, 2013. 3, 4, 5
- [49] L. Zhong, S. Cho, D. Metaxas, S. Paris, and J. Wang. Handling noise in single image deblurring using directional filters. In *CVPR*, 2013. 1, 3, 4